Received: 27 December 2023 | Revised: 30 March 2024 | Accepted: 3 May 2024

DOI: 10.1002/aic.18493

AIChE JOURNAL

RESEARCH ARTICLE

Reaction Engineering, Kinetics and Catalysis

# $CO_2$ absorption mechanism and kinetic modeling of mixed amines with ionic liquid activation

Rui-Qi Jia[1,2] | Qing Wu[3] | Liang-Liang Zhang[1,2] | Bo Zhang[3] | Guang-Wen Chu[1,2] | Jian-Feng Chen[1,2]

[1]Research Center of the Ministry of Education for High Gravity Engineering and Technology, Beijing University of Chemical Technology, Beijing, China

[2]State Key Laboratory of Organic-Inorganic Composites, Beijing University of Chemical Technology, Beijing, China

[3]Institute of Chemicals & Advanced Materials, CNOOC, Beijing, China

**Correspondence**
Liang-Liang Zhang and Guang-Wen Chu, Research Center of the Ministry of Education for High Gravity Engineering and Technology, Beijing University of Chemical Technology, Beijing 100029, China.
Email: zhll@mail.buct.edu.cn and chugw@mail.buct.edu.cn

**Funding information**
National Natural Science Foundation of China, Grant/Award Numbers: 21978011, 22288102

## Abstract

Ionic liquid (IL) can not only serve as solvents to reduce carbon capture energy consumption, but also may activate the $CO_2$ absorption of amine solutions. Here, the absorption mechanism and kinetic modeling of IL-activated single and mixed amines were studied in wetted wall column. N-(2-aminoethyl) ethanolamine (AEEA) and N,N-diethylethanolamine (DEEA) were used as representatives to evaluate the IL activation effects on primary and tertiary amines. It was found that IL activated the reaction process of primary amine, but had no activation effect on tertiary amine. The activation energy of AEEA-IL-$CO_2$ was 22.2 kJ/mol, which was 21.0% lower than AEEA-$CO_2$. Kinetic modeling of IL-activated AEEA and mixed amines was established. Besides, the density functional theory calculations showed that IL can form hydrogen bonding and other interactions with AEEA and $CO_2$ to activate the absorption reaction, which can reduce 29.3% activation energy during the zwitterion formation stage.

**KEYWORDS**
activation, $CO_2$ absorption mechanism, ionic liquid, kinetic modeling, mixed amine

## 1 | INTRODUCTION

Carbon capture, utilization, and storage (CCUS) technology is a supportive measure to achieve the net zero carbon emission target in the future.[1] Chemical absorption, with its well-established process and high gas treatment capacity, has great potential for large-scale commercialization.[2] But high energy consumption remains an obstacle for traditional chemical absorption. To realize a cost-effective carbon capture process, a new generation of absorbents has been widely developed, including phase change absorbents,[3] nanofluid absorbents,[4] ionic liquid absorbents,[5] non-aqueous absorbents.[6]

The typical $CO_2$ absorbent applied in industrial operations is an aqueous solution of organic amines. The main component of traditional amine absorbents is single amines, including monoethanolamine (MEA),[7] N-methyldiethanolamine (MDEA),[8] 2-amino-2-methyl-1-propanol (AMP),[9] and piperazine (PZ),[10] and so forth. Primary or secondary amines have fast absorption ability and high energy cost, whereas tertiary amines have the opposite properties. Therefore, it is important to consider the balance between absorption efficiency and regeneration energy when using a single amine solution. To achieve improved overall performance, mixed amines have been developed, which can achieve the combination of various organic amine characteristics. Mixed amines provide advantages in terms of absorption rate, recycling capacity, and energy savings, such as AMP/PZ,[11] diethanolamine (DEA)/AMP,[12] and MDEA/MEA.[13] It is interesting to note that PZ and DEA can be used as promoters in mixed amines to activate the reaction process and improve the kinetics performance.[14] Furthermore, some mixed amines become attractive for their phase change properties after $CO_2$ absorption, thus expecting further energy savings, for example, N,N-diethylethanolamine (DEEA)/N-(2-aminoethyl) ethanolamine (AEEA), DEEA/1,4-butanediamine (BDA), and DEEA/3-(methylamino)propylamine (MAPA).[15]

  

The presence of water in amine absorbents leads to unavoidably high sensible and latent heat consumption.[16] The replacement of partial water by using an effective solvent with low heat capacity, vapor pressure, and evaporation enthalpy is a feasible strategy to improve absorbent performance. These effective solvents contain alcohols,[17] ethers,[18] ketones,[19] sulfones,[20] ionic liquids,[21] and others. Zhu et al.[18] proposed the MEA/SA (a type of ether)/$H_2O$ system, which has a 43.6% reduction in energy consumption compared to 20 wt% MEA. It was also found that the initial absorption rate was proportional to the SA concentration, which probably resulted from the solvent effect of SA. Jin et al.[22] investigated an absorbent consisting of DEEA/AEEA/n-butanol/$H_2O$ and found that this absorbent had a higher recycling capacity and lower energy consumption than DEEA/AEEA/$H_2O$. The initial absorption rate of the absorbent was increased due to the solvent effect of n-butanol which reduced the influence of polar water molecules on the AEEA absorption process. Therefore, an effective combination of organic amines and other solvents not only improves the $CO_2$ recycling capacity and the energy-saving level of the absorbent, but also has a potential activation effect on the $CO_2$ absorption reaction.

Compared to other solvents, ionic liquids (ILs) as green solvents are more eco-friendly co-solvents for $CO_2$ capture owing to their properties such as extremely low vapor pressure, low corrosivity, and high stability.[23] Meanwhile, ILs have non-volatility and lower specific heat capacity, which contributes to the reduction of sensible and latent heat during the regeneration process. Meng et al.[24] studied the absorption and desorption characteristics of MEA/1-butyl-3-methylimidiazolium tetrafluoroborate ([Bmim][$BF_4$], BF)/$H_2O$ absorbent, which has a 43.2% lower energy consumption than 30 wt% MEA. It was also found that the initial absorption efficiency tended to increase after BF addition. It was attributed the kinetic improvement to the solvent effect of BF which reduced the reaction energy barrier and accelerated the absorption process. When IL co-exists with amine solutions, its influence on $CO_2$ chemical reactions could not be ignored. Lu et al.[25] studied the MEA/BF/$H_2O$ system and speculated that the IL might serve as a base to participate in the deprotonation reaction. Based on the overall kinetic behavior of MDEA/BF/$H_2O$, Ahmady et al.[26] found that an increase in the IL concentration would lead to a decrease in the activation energy, suggesting a possible catalytic effect. As reported in many studies, ILs have an activation effect on $CO_2$ absorption in organic amines. However, the molecular reaction mechanism and kinetic parameters of IL in the organic amine are still unclear and require in-depth research.

The objective of this research is to investigate the activation mechanism of IL in single amines and mixed amines at the molecular level and to establish the IL-activated kinetic modeling. DEEA and AEEA were used as representatives to evaluate the activation effects of IL on tertiary and primary amines, respectively, and their mixtures were chosen as representative of mixed amines. Firstly, the Arrhenius equations of DEEA and AEEA were obtained using a wetted wall column (WWC) apparatus and compared with related reports to verify the experimental feasibility. Then the BF was chosen to represent conventional IL due to its exceptional water solubility and economical production cost.[23] The kinetic data of single amines at different BF concentrations were obtained to propose an IL-activated kinetic model linking to activator concentration. Finally, the parallel reaction model for mixed amines was validated and the IL activation model was used for the mixed amine system. In addition, the energy variation and interaction of the reaction pathways for IL-activated mixed amines were calculated using DFT to reveal the reaction mechanism.

## 2 | METHODOLOGY

### 2.1 | Chemicals

DEEA, AEEA, and BF (≥99% purity) were purchased from Shanghai Macklin Co., Ltd., China. $N_2$ and $CO_2$ (≥99.9% purity) were obtained by Beijing Shun'an Qite Gas Co., Ltd., China.

### 2.2 | Experimental procedure

The experimental procedure is shown in Figure 1. The flue gas is simulated by a mixture of $CO_2$ and $N_2$ gases with the proportion controlled by flow meters. The gas passes through a water bath and enters via the gas inlet at the bottom of the WWC. The absorbent is preheated in the water bath for the specified temperature and then goes into the WWC via the feed pump. The absorbent enters at the bottom of the falling film tube, forms a falling film at the top, and flows down to provide a uniform liquid film on the tube wall, which reacts with the simulated flue gas in reverse contact. After condensation and drying, the outlet gas enters the $CO_2$ analyzer (GXH-3010E1) for testing. The outlet liquid is returned to the absorbent storage tank for recycling. The total simulated flue gas flow rate is set at 1.6 L/min, and the absorbent flow rate is 120 mL/min. The WWC consists of two glass shrouds and a falling film tube. The outer glass shroud maintains a constant temperature in the reactor using a water bath, and the inner glass shroud serves as a space for gas–liquid reactions. The gas–liquid contact area of the WWC is 38.52 $cm^2$. The diameter of the falling film tube is 1.26 cm and the height is 9.1 cm. The experimental temperature range is 293.15–333.15 K.

The density and viscosity of the absorbent were measured using the pyknometer method and viscometer (Shanghai Fangrui Instruments Co., Ltd., China). The diffusion coefficients and Henry's constants were derived using the $N_2O$ analogy method as in Equations (S3) and (S4). The diffusion coefficients and Henry's constants for $CO_2$ and $N_2O$ in water were obtained by empirical formulas in Equations (S5–S8), and diffusion coefficients and Henry's constants for $N_2O$ in amines were calculated by correlation of viscosity and concentration in Equations (S9) and (S10).[27,28] The Henry's constant for the absorbent with IL was corrected by Equation (S11).[29]

### 2.3 | Mass transfer

In WWC, the total mass transfer coefficient ($K_G$) can be obtained from the slope of the mass transfer flux ($N_F$) on the logarithmic average pressure ($P_{CO2}$) as in Equation (1).[30]

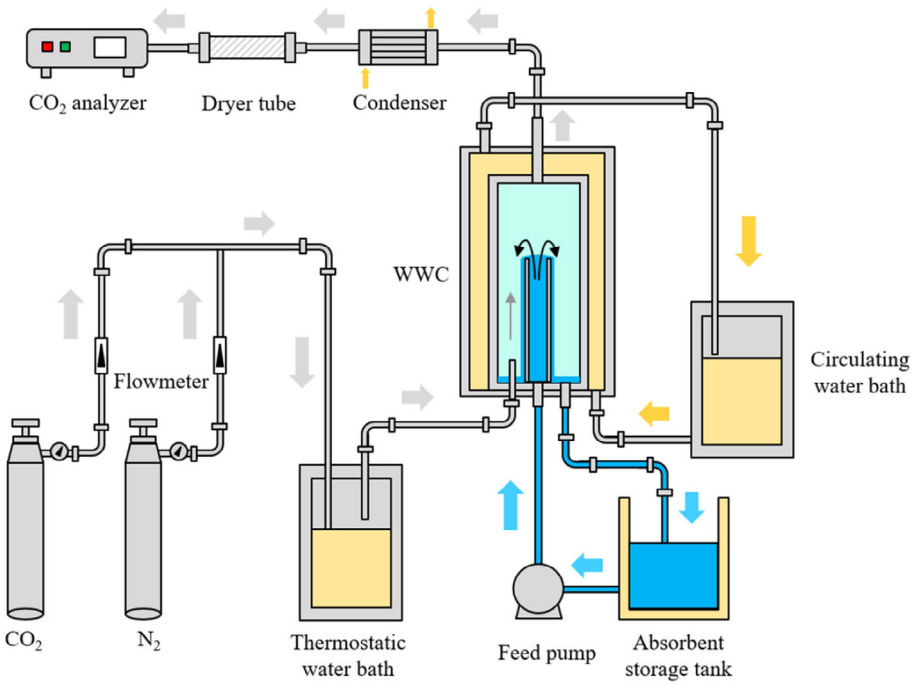


**FIGURE 1** Experimental flowsheet of wetted wall column.

$$N_F = K_G\left(P_{CO_2} - P^*_{CO_2}\right) \tag{1}$$

$N_F$ and $P_{CO2}$ can be calculated by Equations (S1) and (S2), respectively. $P^*_{CO_2}$ is the equilibrium partial pressure. Five different $CO_2$ partial pressures were set for the experiment. Each group of data was measured three times and the average value was used to fit the curve to determine the $K_G$, as shown in Figure S1.

The gas side mass transfer coefficient ($k_g$) is obtained from the Sherwood number (*Sh*) by Equation (2).[31] The Sherwood number is calculated by Equation (3). The Reynolds (*Re*) and Schmidt numbers (*Sc*) are given by Equations (4) and (5), respectively.

$$Sh = \frac{RTk_g d}{D_{CO_2}} \tag{2}$$

$$Sh = 1.075\left(ReSc\frac{d}{h}\right)^{0.85} \tag{3}$$

$$Re = \frac{\rho v d}{\mu} \tag{4}$$

$$Sc = \frac{\mu}{\rho D_{CO_2}} \tag{5}$$

*R* is the gas constant. *T* is the gas temperature. *d* and *h* are the relevant dimensions of the gas-flowing passage. $\rho$, $\mu$, *v*, $D_{CO2}$ are the density, viscosity, flow velocity, and diffusion coefficient of the gas, respectively. The density of gas is obtained by the ideal gas law. The viscosity of gas is given by the correlation equation proposed by Naghizadeh et al.[32] The diffusion coefficient of gas is estimated from the Fuller equation. Corresponding data are given in Table S1.

The physical liquid side mass transfer coefficient ($k_L^0$) is calculated by Equation (6).[33]

$$k_L^0 = \frac{3Q}{A}\sqrt{\frac{\varepsilon}{\pi}} \tag{6}$$

*Q* is the liquid flow rate. *A* is the gas–liquid contact area. The dimensionless number ($\varepsilon$) can be calculated by Equation (7). Liquid surface flow velocity and liquid film thickness are obtained based on Equations (8) and (9).

$$\varepsilon = \frac{D_{CO_2} h}{\nu_{surf}\delta^2} \tag{7}$$

$$\nu_{surf} = \frac{\rho g \delta^2}{2\mu} \tag{8}$$

$$\delta = \sqrt[3]{\frac{3\mu Q}{\rho g L}} \tag{9}$$

*L* and *h* are the relevant dimensions of the falling film tube. $\rho$, $\mu$, *Q*, and $D_{CO2}$ are the density, viscosity, flow rate, and diffusion coefficient of the absorbent, respectively. *g* is the gravitational acceleration.

The relationship between the various mass transfer coefficients in the two-film theory is shown in Equation (10). The liquid side mass transfer coefficient ($k_L$) is given by Equation (11).

$$\frac{1}{k_g} + \frac{1}{k_L} = \frac{1}{K_G} \tag{10}$$

$$\frac{1}{k_L} = \frac{H}{Ek_L^0} \tag{11}$$

*H* is the Henry's constant. The chemical enhancement factor (*E*) approximately equals the Hatta number (*Ha*) in the two-film theory,

as in Equation (12). And the precondition is the fulfillment of the condition (13). The infinite enhancement factor ($E_\infty$) can be defined by Equation (14).[34] *Ha* can be calculated by Equation (15). Therefore, the overall reaction rate constant ($k_{ov}$) can be obtained from Equation (16).[35]

$$E \approx Ha \tag{12}$$

$$3 < Ha < < E_\infty \tag{13}$$

$$E_\infty = 1 + \frac{D_{Amine} C_{Amine}}{2 D_{CO_2} C_{CO_2}} \tag{14}$$

$$Ha = \frac{\sqrt{k_{ov} D_{CO_2}}}{k_L^0} \tag{15}$$

$$k_{ov} = \frac{\left(E k_L^0\right)^2}{D_{CO_2}} \tag{16}$$

$D_{Amine}$ is the diffusion coefficient of amine in liquid phase, which can be obtained by Equation (17).[33] $C_{Amine}$ and $C_{CO2}$ are the concentrations of amine and $CO_2$ in the liquid phase, respectively. $C_{CO2}$ can be calculated using the Henry's law.

$$\ln D_{Amine} = \left(-13.08 + \frac{2360.70}{T} - 24.73 \times 10^{-5} C_{Amine}\right) \frac{M_{Amine}}{M_{MDEA}} \tag{17}$$

## 2.4 | Reaction mechanism

The reaction between tertiary amine and $CO_2$ follows the base-catalyzed hydration mechanism in Equation (18).[36] Thus, the DEEA reaction kinetics can be represented as Equation (19).

$$DEEA + CO_2 + H_2O \overset{k_{DEEA}}{\leftrightarrow} DEEAH^+ + HCO_3^- \tag{18}$$

$$r_{CO_2\text{-}DEEA} = k_{DEEA} C_{DEEA} C_{CO_2} \tag{19}$$

The zwitterions mechanism is considered the reaction mechanism of primary/secondary amines.[30] It consists of two steps, the zwitterion formation stage and the deprotonation stage, as in Equations (20) and (21–25). $B_i$ is the base that traps the proton, including amines, $H_2O$, and $OH^-$. Based on the steady state approximation principle, the kinetic model of AEEA with $CO_2$ can be expressed as Equation (26). As the condition (27) is satisfied, the model can be simplified to Equation (28).

$$CO_2 + AEEA \underset{k_{\text{-}AEEA}}{\overset{k_{AEEA}}{\leftrightarrow}} AEEAH^+COO^- \tag{20}$$

$$AEEAH^+COO^- + B_i \overset{k_{B,i}}{\rightarrow} AEEACOO^- + B_iH^+ \tag{21}$$

$$AEEAH^+COO^- + AEEA \overset{k_{B,AEEA}}{\rightarrow} AEEACOO^- + AEEAH^+ \tag{22}$$

$$AEEAH^+COO^- + DEEA \overset{k_{B,DEEA}}{\rightarrow} AEEACOO^- + DEEAH^+ \tag{23}$$

$$AEEAH^+COO^- + H_2O \overset{k_{B,H_2O}}{\rightarrow} AEEACOO^- + H_3O^+ \tag{24}$$

$$AEEAH^+COO^- + OH^- \overset{k_{B,OH^-}}{\rightarrow} AEEACOO^- + H_2O \tag{25}$$

$$r_{CO_2\text{-}AEEA} = \frac{C_{AEEA} C_{CO_2}}{\frac{1}{k_{AEEA}} + \frac{k_{\text{-}AEEA}}{k_{AEEA} \sum_i k_{B_i} C_{B_i}}} = \frac{k_{AEEA} C_{AEEA} C_{CO_2}}{1 + \frac{k_{\text{-}AEEA}}{\sum_i k_{B_i} C_{B_i}}} \tag{26}$$

$$\sum_i k_{B_i} C_{B_i} > > k_{\text{-}AEEA} \tag{27}$$

$$r_{CO_2\text{-}AEEA} = k_{AEEA} C_{AEEA} C_{CO_2} \tag{28}$$

In addition, the hydration of $CO_2$ and the kinetic formula is denoted as Equations (29–32).

$$H_2O \leftrightarrow H^+ + OH^- \tag{29}$$

$$CO_2 + H_2O \overset{k_{H_2O}}{\leftrightarrow} H^+ + HCO_3^- \tag{30}$$

$$CO_2 + OH^- \overset{k_{OH^-}}{\leftrightarrow} HCO_3^- \tag{31}$$

$$r_{CO_2\text{-}H_2O} = k_{H_2O} C_{H_2O} C_{CO_2} + k_{OH^-} C_{OH^-} C_{CO_2} \tag{32}$$

The total reaction kinetics of the mixed amine can be represented in Equation (33).[37] The $k_{ov}$ is simplified to Equation (35) because of the negligible effect of $OH^-$ and $H_2O$ on the total rate.[38]

$$r_{overall} = (k_{DEEA} C_{DEEA} + k_{AEEA} C_{AEEA} + k_{H_2O} C_{H_2O} + k_{OH^-} C_{OH^-}) C_{CO_2} \tag{33}$$

$$r_{overall} = k_{ov} C_{CO_2} \tag{34}$$

$$k_{ov} = k_{DEEA} C_{DEEA} + k_{AEEA} C_{AEEA} \tag{35}$$

## 2.5 | Simulation method

The energy changes and intermolecular interactions in different reaction paths were simulated on density functional theory (DFT) using the Gaussian 09 package.[39] Geometry optimization, transition state search, intrinsic reaction coordinate (IRC) calculations, and Gibbs free energy calculations were performed at the B3LYP/6-31G(d) and B2PLYPD3/def2TZVP levels. The protocol using different theoretical methods and basis sets to solve the corresponding computational requirements is frequently applied to reduce the computational cost.[40] The general solvation model (SMD) was used to evaluate solvent effects. Multiwfn 3.8 and VMD software were applied for interaction analysis and visualization modeling.[41]

## 3 | RESULTS AND DISCUSSION

### 3.1 | Determination of physical properties

Data on physical properties of density, viscosity, diffusion coefficient, and Henry's constant for different systems are listed in Table S2. The changes in density and viscosity of different systems are shown in Figures 2 and 3. It was worth noting that both density and viscosity decreased with temperature increasing but increased with BF concentration increasing. The addition of IL had a significant effect on density and viscosity, even at low levels. The changes in diffusion coefficient and Henry's constant of different systems are shown in Figures S2 and S3. The diffusion coefficients were positively correlated with the temperature and negatively correlated with the IL concentration, indicating that the high viscosity of IL affected the $CO_2$ diffusion degree in gas–liquid mass transfer. Henry's constant rose as amine concentration increased, and was slightly affected by BF concentration in 0.5–2.0 wt%.

### 3.2 | Kinetics of single amine absorbents

The kinetics of two different types of single amines were first studied at 293.15–333.15 K to verify the stability and reliability of the experimental method. The concentrations of DEEA and AEEA were set at 10 and 5 wt%. Detailed data on mass transfer and kinetics of $CO_2$ absorption for DEEA and AEEA are listed in Table S3. The $K_G$ of the AEEA absorbent was much higher than that of DEEA by about 6–10 times. Meanwhile, the $E_\infty$ was sufficiently greater than *Ha* in all the experimental conditions, satisfying Equation (13). In this case, the gas–liquid reaction was in accordance with the two-film theory and was suitable for a fast pseudo-primary reaction, and *E* was approximately equal to *Ha*.[42] Then the $k_{ov}$ of two single amine solutions at different temperatures could be obtained by Equation (16). The $k_{ov}$ of AEEA was much larger than that of DEEA due to the difference in the amine groups.

According to the kinetic modeling of DEEA and AEEA in Equations (19) and (28), the kinetic rate constants $k_{DEEA}$ and $k_{AEEA}$ can be determined by excluding the concentration effect. A comparison of $k_{DEEA}$ and $k_{AEEA}$ with values reported in the literature is shown in Figure 4. The $k_{DEEA}$ agreed well with that reported by Li et al.,[43] but slightly higher than the values reported by Little et al.,[44] Kierzkowska-Pawlak,[45] Benitez-Garcia et al.[46] The dispersion of kinetic data may be explained by differences in measurement equipment.[47] Other researchers used stopped-flow equipment, stirred cell reactor, and wetted-sphere apparatus, respectively. The $k_{AEEA}$ was close to the literature values of Kierzkowska-Pawlak et al.,[42] Manun et al.,[48]

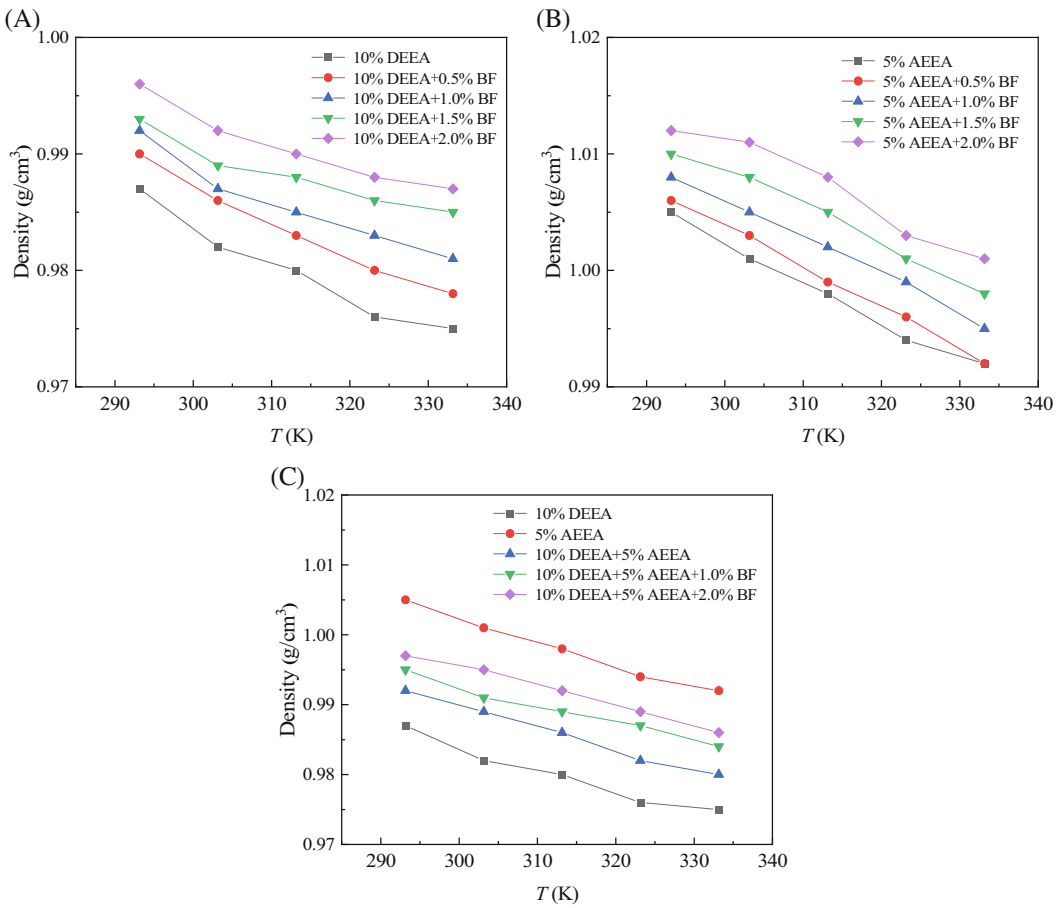


**FIGURE 2** Densities of different systems. (A) DEEA + BF; (B) AEEA + BF; (C) DEEA + AEEA + BF.

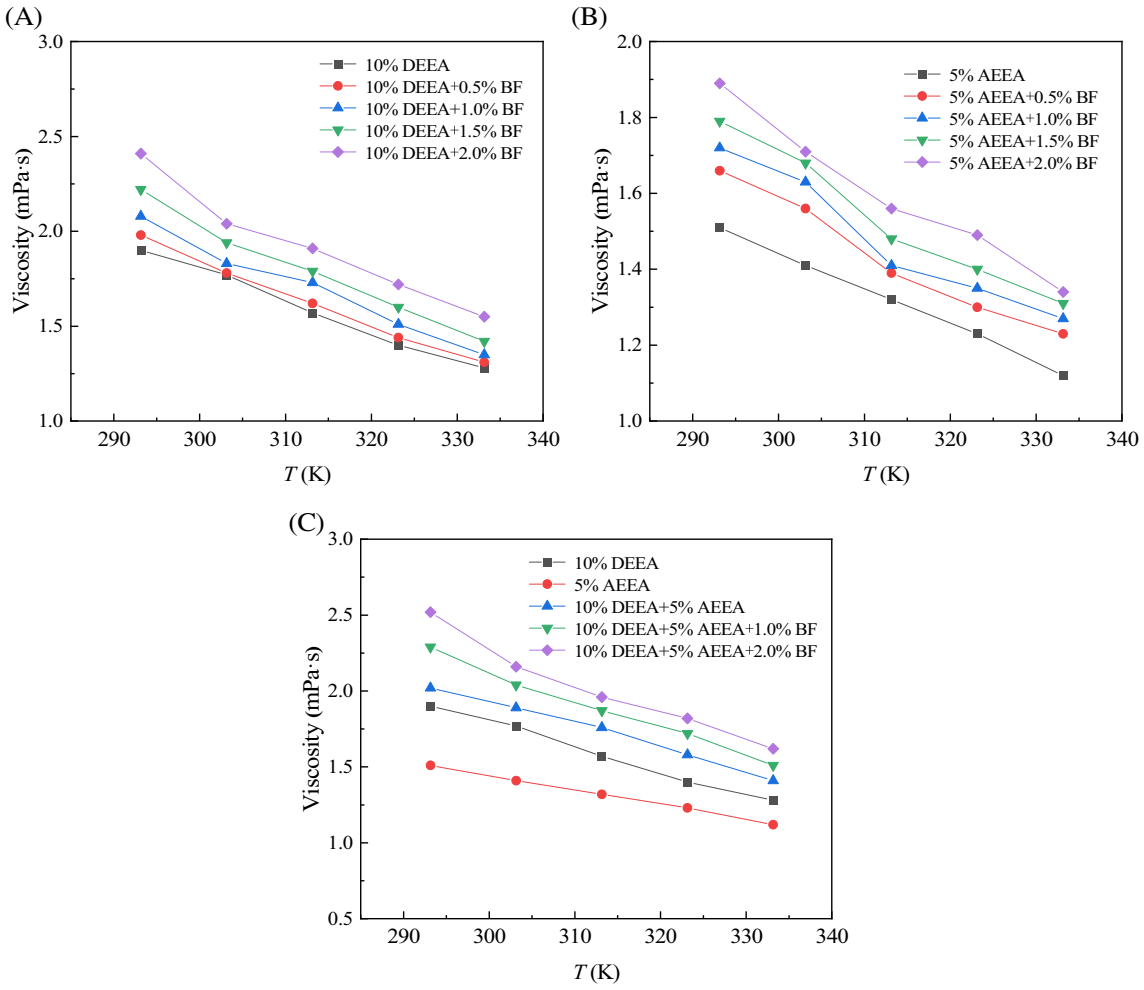


**FIGURE 3** Viscosities of different systems. (A) DEEA + BF; (B) AEEA + BF; (C) DEEA + AEEA + BF.

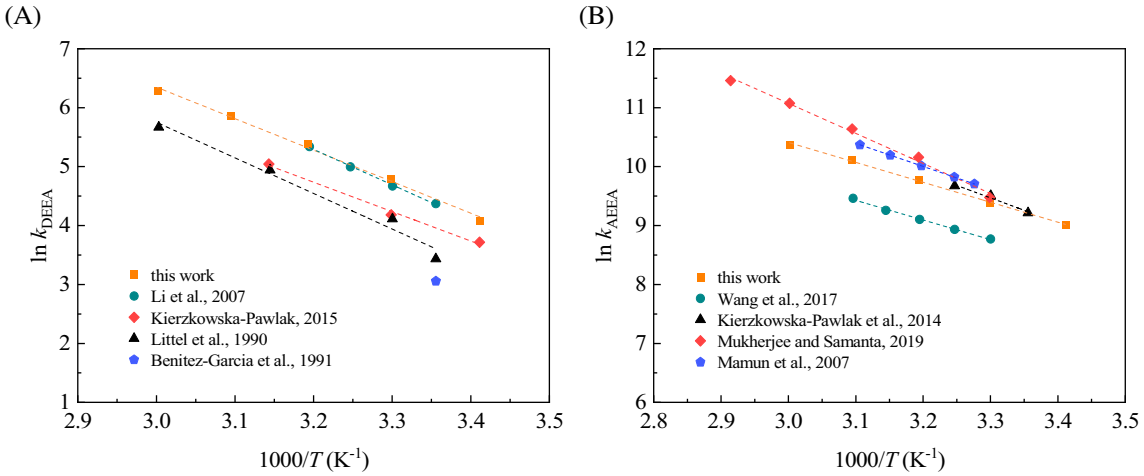


**FIGURE 4** A comparison with the $k_{DEEA}$ and $k_{AEEA}$ reported by others. (A) DEEA; (B) AEEA.

Mukherjee and Samanta,[49] and slightly larger than the values in Wang et al.,[33] which might be because of the different experimental conditions and mass transfer correlation equation. The Sherwood number calculation equation used in this study was not the same as that of Wang et al. In addition, different estimation methods for the relevant physical parameters might also account for the small differences.

Based on the Arrhenius equation, the logarithm of the rate constant (ln*k*) correlation equation was fitted with the reciprocal of temperature (1000/*T*), which showed a linear dependence in Figure S4. The Arrhenius equation for $k_{DEEA}$ and $k_{AEEA}$ were given in Equations (36) and (37). Therefore, the reaction activation energies of DEEA-$CO_2$ and AEEA-$CO_2$ were 44.4 and 28.1 kJ/mol, respectively.

$$k_{DEEA} = 5.26 \times 10^9 \exp\left(-\frac{5344.89}{T}\right),\ \mathrm{L \cdot mol^{-1} \cdot s^{-1}} \quad (36)$$

**TABLE 1** Mass transfer and kinetic data for DEEA and AEEA with BF.

| Absorbent | *T* (K) | $K_G$ ($10^{-11}$ mol/(cm$^2$ s Pa)) | $k_g$ ($10^{-9}$ mol/(cm$^2$ s Pa)) | $k_L^0$ ($10^{-3}$ cm/s) | *Ha* | $k_{ov}$ ($s^{-1}$) | $E_\infty$ |
|---|---|---|---|---|---|---|---|
| 10%DEEA + 0.5%BF | 293.15 | 0.81 | 2.57 | 5.45 | 9.37 | 53.81 | 185.68 |
| | 303.15 | 1.09 | 2.52 | 6.52 | 13.01 | 107.26 | 216.24 |
| | 313.15 | 1.34 | 2.47 | 7.69 | 16.63 | 180.77 | 250.55 |
| | 323.15 | 1.68 | 2.43 | 9.12 | 21.33 | 308.99 | 281.04 |
| | 333.15 | 1.94 | 2.39 | 10.62 | 25.33 | 449.34 | 317.16 |
| 10%DEEA + 1.0%BF | 293.15 | 0.79 | 2.57 | 5.30 | 9.43 | 53.67 | 193.86 |
| | 303.15 | 1.07 | 2.52 | 6.42 | 13.05 | 106.99 | 221.76 |
| | 313.15 | 1.32 | 2.47 | 7.41 | 17.13 | 187.70 | 264.70 |
| | 323.15 | 1.64 | 2.43 | 8.88 | 21.42 | 307.06 | 292.51 |
| | 333.15 | 1.95 | 2.39 | 10.44 | 25.94 | 466.75 | 325.45 |
| 10%DEEA + 1.5%BF | 293.15 | 0.73 | 2.57 | 5.11 | 9.00 | 47.79 | 204.98 |
| | 303.15 | 0.98 | 2.52 | 6.21 | 12.38 | 94.57 | 233.05 |
| | 313.15 | 1.34 | 2.47 | 7.27 | 17.77 | 199.83 | 272.69 |
| | 323.15 | 1.57 | 2.43 | 8.60 | 21.18 | 294.58 | 306.98 |
| | 333.15 | 1.92 | 2.39 | 10.16 | 26.35 | 474.41 | 339.44 |
| 10%DEEA + 2.0%BF | 293.15 | 0.74 | 2.57 | 4.88 | 9.59 | 52.86 | 219.68 |
| | 303.15 | 1.00 | 2.52 | 6.04 | 12.99 | 102.48 | 243.34 |
| | 313.15 | 1.28 | 2.47 | 7.01 | 17.55 | 190.98 | 287.91 |
| | 323.15 | 1.48 | 2.43 | 8.26 | 20.83 | 278.28 | 325.90 |
| | 333.15 | 1.83 | 2.39 | 9.67 | 26.33 | 460.26 | 364.66 |
| 5%AEEA + 0.5%BF | 293.15 | 9.24 | 2.57 | 6.04 | 95.18 | 5916.83 | 918.58 |
| | 303.15 | 9.97 | 2.52 | 7.05 | 109.70 | 8016.66 | 1056.12 |
| | 313.15 | 11.18 | 2.47 | 8.41 | 126.92 | 11136.76 | 1255.84 |
| | 323.15 | 11.79 | 2.43 | 9.69 | 140.85 | 14010.26 | 1430.71 |
| | 333.15 | 12.51 | 2.39 | 11.03 | 157.58 | 17839.67 | 1627.19 |
| 5%AEEA + 1.0%BF | 293.15 | 9.36 | 2.57 | 5.92 | 98.79 | 6304.21 | 997.22 |
| | 303.15 | 10.07 | 2.52 | 6.88 | 113.98 | 8534.00 | 1176.50 |
| | 313.15 | 11.36 | 2.47 | 8.34 | 130.36 | 11704.33 | 1273.71 |
| | 323.15 | 12.08 | 2.43 | 9.49 | 147.87 | 15265.22 | 1477.85 |
| | 333.15 | 12.58 | 2.39 | 10.84 | 161.63 | 18588.85 | 1672.49 |
| 5%AEEA + 1.5%BF | 293.15 | 9.49 | 2.57 | 5.79 | 102.86 | 6747.96 | 1033.75 |
| | 303.15 | 10.14 | 2.52 | 6.76 | 117.07 | 8922.63 | 1209.25 |
| | 313.15 | 11.46 | 2.47 | 8.12 | 135.52 | 12459.86 | 1327.59 |
| | 323.15 | 12.13 | 2.43 | 9.30 | 151.85 | 15915.03 | 1524.85 |
| | 333.15 | 12.76 | 2.39 | 10.65 | 167.26 | 19720.90 | 1717.69 |
| 5%AEEA + 2.0%BF | 293.15 | 9.56 | 2.57 | 5.62 | 107.29 | 7215.03 | 1084.07 |
| | 303.15 | 10.26 | 2.52 | 6.70 | 120.09 | 9342.24 | 1230.53 |
| | 313.15 | 11.58 | 2.47 | 7.89 | 141.51 | 13362.93 | 1388.39 |
| | 323.15 | 12.25 | 2.43 | 8.98 | 159.34 | 17174.97 | 1606.31 |
| | 333.15 | 12.84 | 2.39 | 10.52 | 170.78 | 20424.60 | 1752.34 |

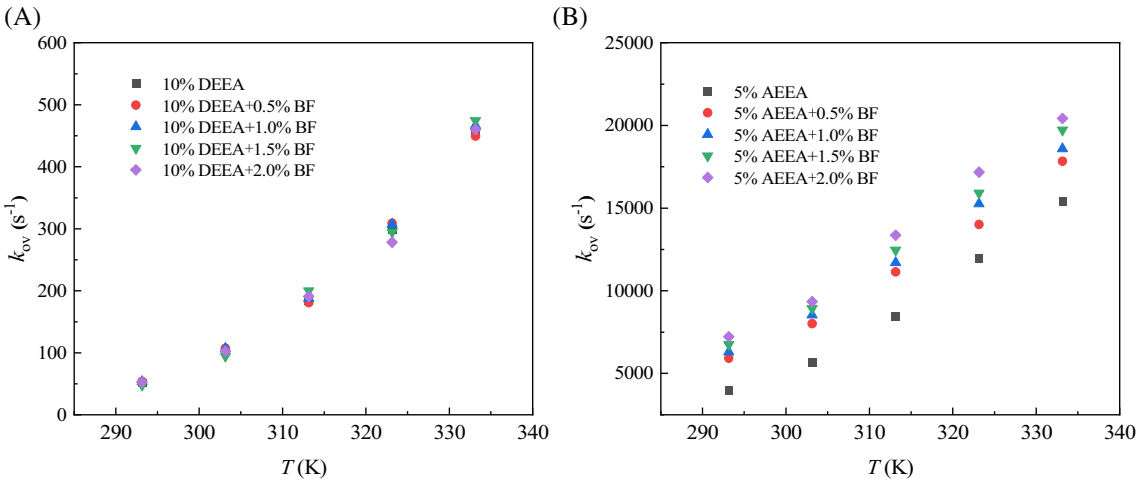


**FIGURE 5** The $k_{ov}$ at different IL concentrations. (A) DEEA; (B) AEEA.

$$k_{AEEA} = 8.49 \times 10^8 \exp\left(-\frac{3383.23}{T}\right),\ \mathrm{L \cdot mol^{-1} \cdot s^{-1}} \quad (37)$$

### 3.3 | Kinetics of single amine absorbents with ionic liquid activation

The feasibility of the experimental method was determined by single amine kinetics, and then the kinetic research of single amine with IL was performed at the same temperature range. The BF concentrations were in the range of 0.5–2.0 wt%. The results of mass transfer and kinetics of DEEA and AEEA absorbents at different IL concentrations are shown in Table 1. It could be seen that the addition of BF had no effect on the $K_G$ of tertiary amine solvent, while the BF facilitated the increase of $K_G$ in primary amine solvent. The variation rule of $E$ was the same as that of $K_G$, which indicated that the BF might have a function of promoting the $CO_2$ chemical reaction in primary amine.

Analogous to the $k_{ov}$ calculation for single amines, the $k_{ov}$ for different BF concentrations in DEEA and AEEA were calculated in Figure 5. It is important to note that when BF was co-mixed with DEEA, the BF only served as a solvent and had no influence on the chemical reaction of tertiary amine with $CO_2$. In contrast, when BF was blended with AEEA, $k_{ov}$ positively correlated with the IL concentration. The effect of IL on the $k_{ov}$ of different types of amines suggested that IL could activate the $CO_2$ reaction of primary amines, but not the tertiary amines. This phenomenon was determined by the difference in the amine groups, probably due to hydrogen bonding. The primary amine group could provide hydrogen atoms to become a hydrogen bond donor, while the tertiary amine has no excess hydrogen atoms. Therefore, the kinetic modeling of AEEA with BF activation can be modified as Equation (38).

$$r_{CO_2\text{-AEEA-BF}} = k_{AEEA,act} C_{AEEA} C_{CO_2} \quad (38)$$

The effect of BF concentration on AEEA kinetics was further investigated. The Arrhenius equations for the AEEA-$CO_2$ reaction at different BF concentrations were determined in Figure 6. The slopes were similar at different concentrations and the intercepts were different. This indicated that the activation energy was the same in the presence of IL and the activation degree was variable. Catalyst concentration can be empirically related to the Arrhenius equation and correlated with the frequency factor.[50,51] We introduced the activator concentration ($C_{act}$), the concentration ratio of activator to reactant, to modify the Arrhenius equation in Equation (39) so as to exhibit the activation effect of IL in amine solutions.

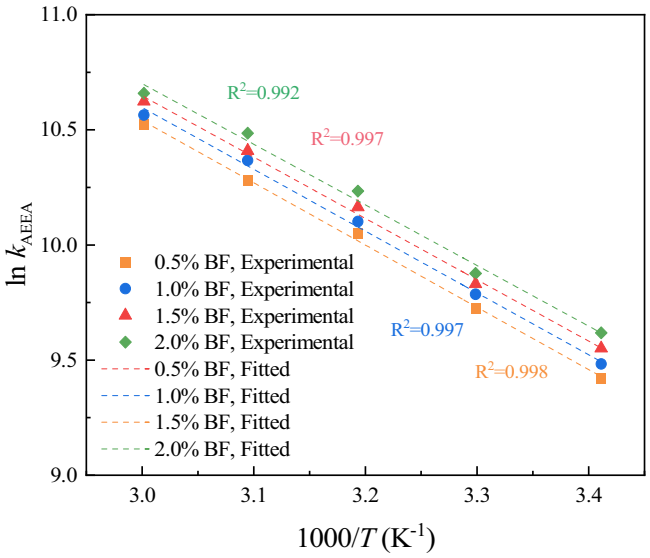


**FIGURE 6** Kinetic experimental data and fitting of single amine solutions with IL.

$$k_{AEEA,act} = \alpha C_{act}{}^{\beta} e^{\frac{-E_a}{RT}} \quad (39)$$

The Arrhenius equation for the AEEA with BF activation was obtained by regression fitting in the form of Equation (40), as in

Equation (41). The standard error was 3.0%. The activation energy of AEEA-BF-$CO_2$ was 22.2 kJ/mol, which was 21.0% lower than that of AEEA-$CO_2$. The kinetic modeling results indicate that IL addition reduces the activation energy of AEEA in the $CO_2$ absorption reaction and increases the reaction rate constant.

$$\ln k_{AEEA,act} = \frac{-E_a}{RT} + \beta \ln C_{act} + \ln \alpha \quad (40)$$

$$k_{AEEA,act} = 1.64 \times 10^8 C_{act}^{0.1221} e^{\frac{-2672.37}{T}} \quad (41)$$

## 3.4 | Kinetics of mixed amine absorbents with ionic liquid activation

The kinetic modeling of mixed amines can be described using a parallel reaction mechanism as in Equation (35). We found that IL can activate the absorption kinetics of primary amines and reduce the reaction activation energy, but without this effect in tertiary amines. Thus, combining Equations (35) and (38), the kinetic modeling for mixed amines under BF activation can be expressed as Equation (42). Kinetic experiments with mixed amines at different BF concentrations were performed to validate the reliability of the model. The concentrations of DEEA and AEEA remained constant at 10 and 5 wt%. The BF concentrations were 1–2 wt%. The predicted $k_{ov}$ of the model was calculated by Equations (36), (37), and (41).

$$k_{ov} = k_{DEEA} C_{DEEA} + k_{AEEA,act} C_{AEEA} \quad (42)$$

The conventional mixed amine model for DEEA/AEEA is first validated and the kinetic data are presented in Table 2. The correlation between experimental and modeled $\ln k_{ov}$-1000/$T$ is in Figure 7. The model error was within 7% in Figure S5, suggesting that the parallel reaction model was suitable for the DEEA/AEEA mixed amine system.

Kinetic data for the mixed amine system with BF activation are similarly presented in Table 2. The result obtained by the IL activation model was compared with the experiment results in Figure 8. The model error was within 8% in Figure 9. Thus, the IL activation model is also applicable to the mixed amine system with reliability in predicting the kinetic properties. In addition, to understand in depth the mechanism of IL for $CO_2$ absorption reaction, quantum chemistry is needed to determine the energy changes and interactions of the reaction paths.

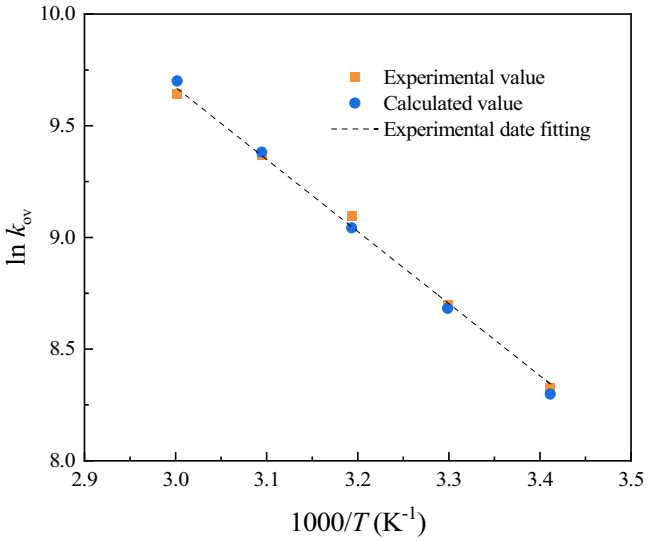


**FIGURE 7** Validation of mixed amine kinetic modeling.

**TABLE 2** Mass transfer and kinetic data for mixed amines with BF.

| Absorbent | $T$ (K) | $K_G$ ($10^{-11}$ mol/(cm$^2$ s Pa)) | $k_g$ ($10^{-9}$ mol/(cm$^2$ s Pa)) | $k_L^0$ ($10^{-3}$ cm/s) | $Ha$ | $k_{ov}$ (s$^{-1}$) | $E_\infty$ |
|---|---|---|---|---|---|---|---|
| 10%DEEA + 5%AEEA | 293.15 | 6.60 | 2.57 | 5.39 | 82.44 | 4138.98 | 582.85 |
| | 303.15 | 7.37 | 2.52 | 6.31 | 98.08 | 5983.19 | 695.18 |
| | 313.15 | 8.42 | 2.47 | 7.34 | 118.52 | 8938.39 | 814.03 |
| | 323.15 | 9.20 | 2.43 | 8.66 | 133.35 | 11713.63 | 913.51 |
| | 333.15 | 10.14 | 2.39 | 10.19 | 150.03 | 15388.69 | 1008.03 |
| 10%DEEA + 5%AEEA + 1.0%BF | 293.15 | 7.71 | 2.57 | 5.02 | 104.59 | 6394.85 | 649.14 |
| | 303.15 | 8.53 | 2.52 | 6.04 | 119.79 | 8706.21 | 743.39 |
| | 313.15 | 9.49 | 2.47 | 7.09 | 139.44 | 12137.00 | 858.66 |
| | 323.15 | 10.41 | 2.43 | 8.26 | 159.56 | 16328.80 | 981.64 |
| | 333.15 | 10.82 | 2.39 | 9.81 | 167.33 | 18735.28 | 1068.42 |
| 10%DEEA + 5%AEEA + 2.0%BF | 293.15 | 7.86 | 2.57 | 4.76 | 113.39 | 7285.12 | 705.95 |
| | 303.15 | 8.69 | 2.52 | 5.85 | 126.76 | 9578.26 | 782.82 |
| | 313.15 | 9.71 | 2.47 | 6.91 | 147.42 | 13367.73 | 895.93 |
| | 323.15 | 10.66 | 2.43 | 8.00 | 169.58 | 18111.97 | 1031.18 |
| | 333.15 | 11.04 | 2.39 | 9.43 | 178.45 | 20828.33 | 1134.04 |

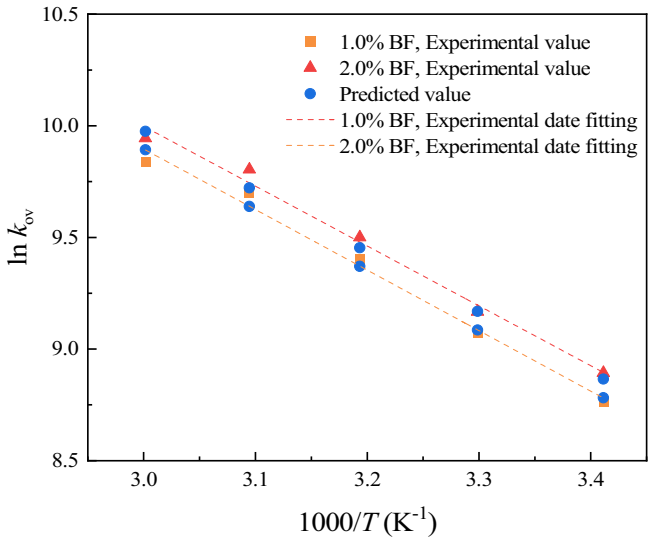


**FIGURE 8** Validation of mixed amine kinetic modeling for IL activation.

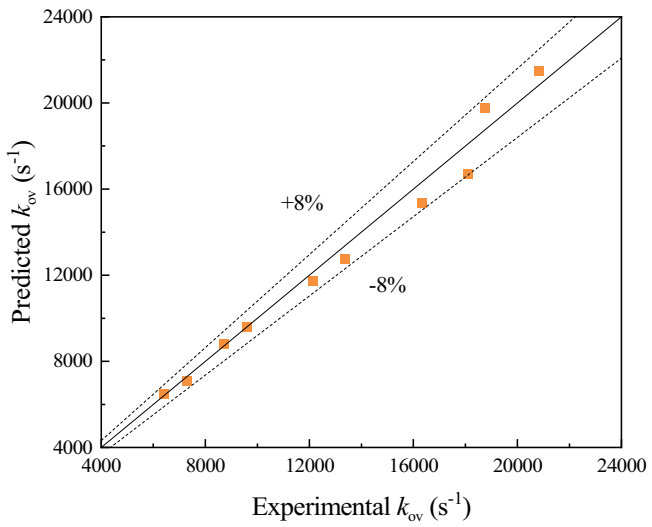


**FIGURE 9** Comparison of experimental values with model predictions.

## 3.5 | Reaction pathway and intermolecular interaction mechanism

For further investigation of the activation mechanism by IL, the reaction pathways and molecular interactions in DEEA/AEEA/BF were studied through DFT calculations. The simulations were performed with AEEA as the main reactant. To indicate the energy changes, the sum of the Gibbs free energies of the reactant monomers for each reaction is set as the benchmark. The Gibbs free energy changes and molecular structures of each reaction pathway are presented in Figure 10.

The $CO_2$ absorption process was simulated in two stages, including the zwitterion formation and the deprotonation process. It was found that IL activation contributed to the zwitterion formation stage. The comparison of the zwitterion formation with and without BF is in Table 3. The reaction activation energy was reduced by 29.3% from 18.4 to 13.0 kJ/mol in the existence of BF. During the formation of zwitterion, structural demand in $CO_2$ is an important factor contributing to the energy changes, accounting for about 97% of the reactant energy loss.[52] Moreover, the bond angle of $CO_2$ decreased as the amine formed zwitterion with $CO_2$. The smaller the bond angle the higher the required energy delivery. In the presence of BF, the initial bond angle changed little and the transition state bond angle increased by 3.17°, indicating that BF promoted a decrease in the energy required to reach the transition state and thus a lower activation energy was achieved. Based on a similar principle, the distance between the N atom of the amine group and the C atom of the $CO_2$ group was larger in the transition state when BF was involved, and hence the energy penalty was lower.

Meanwhile, the deprotonation process involving three bases ($H_2O$, DEEA, and AEEA) was also analyzed in Figure 11. All three types of deprotonation reactions were proton transfer processes. Among them, DEEA and AEEA were single proton transfer reactions, while water exhibited double proton transfer, which is consistent with the report of Aso et al.[53] The reaction activation energy of amines was much lower than that of water, demonstrating a higher priority for amines to acquire protons.

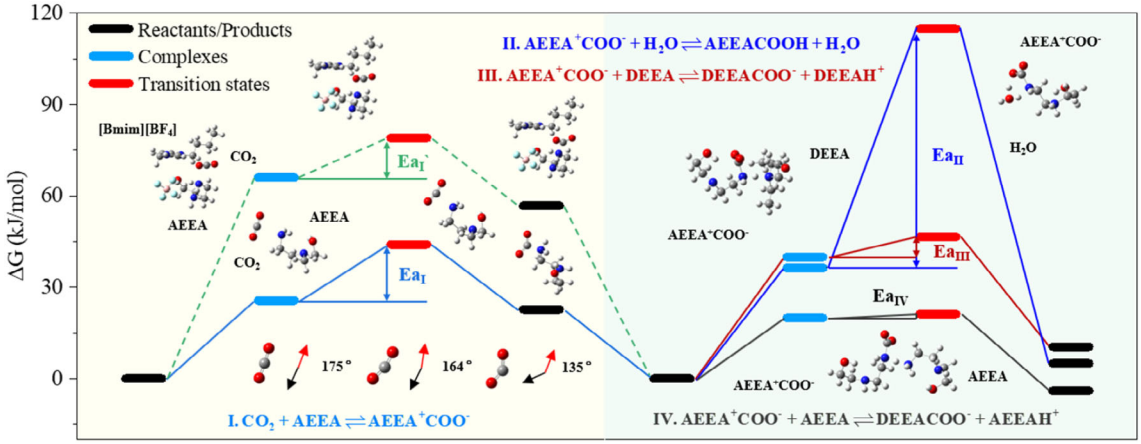


**FIGURE 10** Gibbs free energy changes for $CO_2$ absorption of DEEA/AEEA/BF.

**TABLE 3** Comparison of structure and energy in the zwitterion formation process.

| Reaction | AEEA-$CO_2$ | AEEA-BF-$CO_2$ |
|---|---|---|
| $E_a$ (kJ/mol) | 18.41 | 13.02 |
| $\alpha_{rea}$(°) | 175.60 | 174.62 |
| $\alpha_{ts}$(°) | 161.17 | 164.34 |
| $\alpha_{pro}$(°) | 136.02 | 134.65 |
| C–$N_{rea}$ (Å) | 2.90 | 2.84 |
| C–$N_{ts}$ (Å) | 2.30 | 2.41 |
| C–$N_{pro}$ (Å) | 1.61 | 1.58 |

*Note*: "$_{rea}$": at the reaction state; "$_{ts}$": at the transition state; "$_{pro}$": at the product state 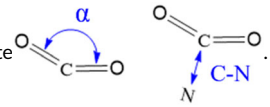


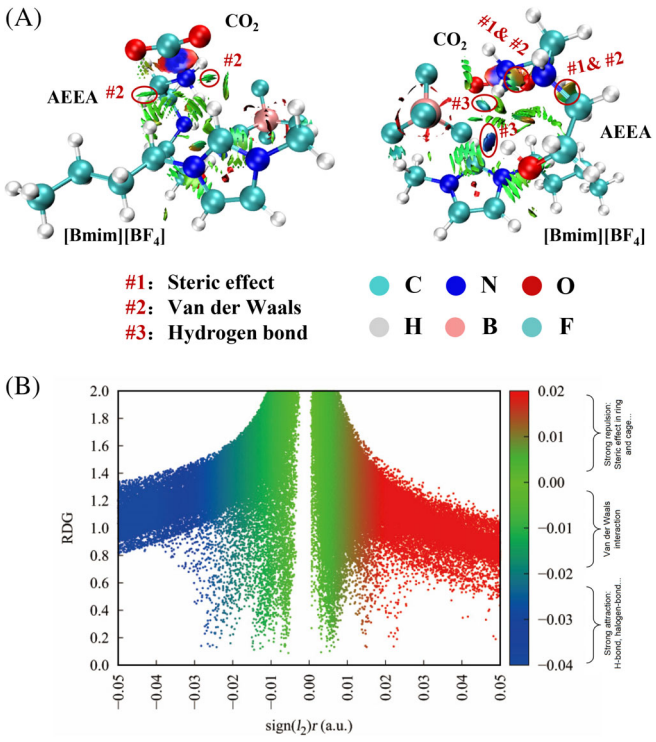


**FIGURE 11** Interaction between [Bmim][$BF_4$] and AEEA in $CO_2$ absorption. (A) Gradient isosurfaces; (B) Scatterplots of the RDG versus sign($l_2$)r function.

The Reduced Density Gradient (RDG) method was applied to analyze the intermolecular interactions of AEEA-BF-$CO_2$ as seen in Figure 11. It was seen that the imidazole cation in BF could form strong Van der Waals interactions with $CO_2$, and the anion could act with the amine group and the hydroxyl group to form hydrogen bonding interactions. The imidazole ring can activate $CO_2$ by forming electrostatic interactions and Lewis acid–base interactions with $CO_2$.[54,55] Anions in BF can weaken the N-H bond by forming hydrogen bonds with the amine group, which promotes the attack of N atoms on $CO_2$ to create zwitterion.[56] Thus, the multiple intermolecular interactions of BF promote the absorption process of AEEA with $CO_2$ and lessen the reaction energy barrier.

## 4 | CONCLUSIONS

In this work, the reaction mechanism and kinetic modeling for IL-activated $CO_2$ absorption of single and mixed amines was investigated. Firstly, the kinetics of single amines were determined to verify the stability and reliability of the experimental methodology. The results showed that the Arrhenius equations for single amines agreed with those reported in the literature. The reaction activation energies for DEEA and AEEA were 44.4 kJ/mol and 28.1 kJ/mol, respectively. Then the kinetic experiments were carried out on single amines with different BF concentrations. A kinetic modeling of IL-activated AEEA was established, and an empirical formula relating the activator concentration to the Arrhenius equation was fitted. The activation energy of IL-activated AEEA was 22.2 kJ/mol, which was reduced by 21.0%. Furthermore, BF was found to have no activation effect on tertiary amines. A parallel reaction model for mixed amines was validated and a good agreement was achieved between the experimental results and the model predictions for the kinetics of IL-activated mixed amines, within an error of 8%. Finally, the reaction pathways and interactions in the DEEA/AEEA/BF system were further investigated by DFT calculations. The simulation results revealed that the activation of BF occurred at the zwitterion formation stage, which led to an increase in the $CO_2$ bond angle and C-N distance of the transition state, and the activation energy could be reduced by 29.3%. The IL could interact with primary amines in several ways, including hydrogen bonding, Van der Waals forces, and Lewis acid–base interactions, as analyzed by RDG. These intermolecular interactions would activate the $CO_2$ absorption reaction, which was the reason for lowering the activation energy and increasing the reaction rate.

### AUTHOR CONTRIBUTIONS

**Rui-Qi Jia:** Investigation (lead); methodology (lead); writing – original draft (lead). **Qing Wu:** Data curation (equal); writing – review and editing (equal). **Liang-Liang Zhang:** Project administration (equal); writing – review and editing (equal). **Bo Zhang:** Writing – review and editing (equal). **Guang-Wen Chu:** Conceptualization (equal); supervision (equal); validation (equal). **Jian-Feng Chen:** Supervision (equal); validation (equal).

### ACKNOWLEDGMENTS

This work was supported by the National Natural Science Foundation of China (Nos. 22288102 and 21978011).

### DATA AVAILABILITY STATEMENT

All data in this research are included in the article itself or the Supplementary Material. The numerical data in Figures 2–10 are available in Tables S2–S7. Input files for the simulations are provided in a folder (Supplementary Review Files-Input Files for Simulations.zip).

The data that support the findings of this study are available from the corresponding author upon reasonable request.

## ORCID

*Liang-Liang Zhang* https://orcid.org/0000-0002-6812-6860

*Guang-Wen Chu* https://orcid.org/0000-0002-3047-7024

## REFERENCES

1. Cao Y, Yang C, Wang C, et al. Evaluation of the rapid phase change absorbents based on potassium glycinate for $CO_2$ capture. *Chem Eng Sci*. 2023;273:118627.
2. Nwaoha C, Idem R, Supap T, et al. Heat duty, heat of absorption, sensible heat and heat of vaporization of 2-amino-2-methyl-1-propanol (AMP), piperazine (PZ) and monoethanolamine (MEA) tri–solvent blend for carbon dioxide ($CO_2$) capture. *Chem Eng Sci*. 2017;170:26-35.
3. Ye J, Jiang C, Chen H, et al. Novel biphasic solvent with tunable phase separation for $CO_2$ capture: role of water content in mechanism, kinetics, and energy penalty. *Environ Sci Technol*. 2019;53(8):4470-4479.
4. Alivand MS, Mazaheri O, Wu Y, Stevens GW, Scholes CA, Mumford KA. Preparation of nanoporous carbonaceous promoters for enhanced $CO_2$ absorption in tertiary amines. *Engineering*. 2020;6(12):1381-1394.
5. Zhu R, Gui C, Li G, Lei Z. Modified COSMO-UNIFAC model for ionic liquid-$CO_2$ systems and molecular dynamic simulation. *AIChE J*. 2022;68(7):e17724.
6. Wang R, Zhao H, Yang X, et al. Energy-efficient non-aqueous biphasic solvent for carbon capture: absorption mechanism, phase evolution process, and non-corrosiveness. *Energy*. 2023;281:128353.
7. Zhang Z, Borhani TN, Olabi AG. Status and perspective of $CO_2$ absorption process. *Energy*. 2020;205:118057.
8. Yang F, Jin X, Fang J, et al. Development of $CO_2$ phase change absorbents by means of the cosolvent effect. *Green Chem*. 2018;20(10):2328-2336.
9. Iliuta I, Bougie F, Iliuta MC. $CO_2$ removal by single and mixed amines in a hollow-fiber membrane module-investigation of contactor performance. *AIChE J*. 2015;61(3):955-971.
10. Liu F, Qi Z, Fang M, Wang T, Yi N. Evaluation on water balance and amine emission in $CO_2$ capture. *Int J Greenh Gas Control*. 2021;112:103487.
11. Zhao D, Xiao X, Wang S, Li M, Liu H. Comprehensive analysis of thermodynamic models forCO2absorption into a blended N,N-diethylethanolamine-1,6-hexamethyl diamine (DEEA-HMDA) amine. *AIChE J*. 2023;69(10):e18174.
12. Zhao Y, Zhang Y, Liu Q, et al. Energy-efficient carbon dioxide capture using piperazine (PZ) activated EMEA + DEEA water lean solvent: performance and mechanism. *Sep Purif Technol*. 2023;316:123761.
13. Jiang W, Luo X, Gao H, et al. A comparative kinetics study of $CO_2$ absorption into aqueous DEEA/MEA and DMEA/MEA blended solutions. *AIChE J*. 2018;64(4):1350-1358.
14. Mesbah M, Momeni M, Soroush E, Shahsavari S, Galledari SA. Theoretical study of $CO_2$ separation from $CO_2$/$CH_4$ gaseous mixture using 2-methylpiperazine-promoted potassium carbonate through hollow fiber membrane contactor. *J Environ Chem Eng*. 2019;7(1):102781.
15. Liu F, Fang M, Yi N, Wang T, Wang Q. Biphasic behaviors and regeneration energy of a 2-(diethylamino)-ethanol and 2-((2-aminoethyl) amino) ethanol blend for $CO_2$ capture. *Sustain Energ Fuels*. 2019;3(12):3594-3602.
16. Zhou X, Li X, Wei J, Fan Y, Liao L, Wang H. Novel nonaqueous liquid-liquid biphasic solvent for energy-efficient carbon dioxide capture with low corrosivity. *Environ Sci Technol*. 2020;54(24):16138-16146.
17. Li X, Liu J, Jiang W, et al. Low energy-consuming $CO_2$ capture by phase change absorbents of amine/alcohol/$H_2O$. *Sep Purif Technol*. 2021;275:119181.
18. Zhu K, Lu H, Liu C, et al. Investigation on the phase-change absorbent system MEA + solvent a (SA) + $H_2O$ used for the $CO_2$ capture from flue gas. *Ind Eng Chem Res*. 2019;58(9):3811-3821.
19. Liu F, Shen Y, Shen L, et al. Novel amino-functionalized ionic liquid/organic solvent with low viscosity for $CO_2$ capture. *Environ Sci Technol*. 2020;54(6):3520-3529.
20. Lv J, Liu S, Ling H, et al. Development of a promising biphasic absorbent for postcombustion $CO_2$ capture: sulfolane + 2-(methylamino) ethanol + $H_2O$. *Ind Eng Chem Res*. 2020;59(32):14496-14506.
21. Xu L, Wang S. Density, viscosity, and $N_2O$ solubility of aqueous solutions of MEA, Bmim$BF_4$, and their mixtures from 293.15 to 333.15 K. *J Chem Eng Data*. 2018;63(8):2708-2717.
22. Jin L, Hou X, Zhan L, et al. Tuning and optimization of two-phase absorbents (DEEA/AEEA/$H_2O$) with hybrid phase splitter (n-butanol/DEEA) for several properties: carbon capture, phase separation, physical properties. *Energy*. 2024;288:129802.
23. Jia R-Q, Xu Y-H, Zhang J-J, Zhang L-L, Chu G-W, Chen J-F. A novel phase change absorbent with ionic liquid as promoter for low energy-consuming $CO_2$ capture. *Sep Purif Technol*. 2023;315:123740.
24. Meng F, Ju T, Han S, et al. Novel monoethanolamine absorption using ionic liquids as phase splitter for $CO_2$ capture in biogas upgrading: high $CH_4$ purity and low energy consumption. *Chem Eng J*. 2023;462:142296.
25. Lu B, Wang X, Xia Y, Liu N, Li S, Li W. Kinetics of carbon dioxide absorption into mixed aqueous solutions of MEA + [Bmim]$BF_4$ using a double stirred cell. *Energy Fuel*. 2013;27(10):6002-6009.
26. Ahmady A, Hashim MA, Aroua MK. Kinetics of carbon dioxide absorption into aqueous MDEA + [bmim][$BF_4$] solutions from 303 to 333K. *Chem Eng J*. 2012;200-202:317-328.
27. Saha AK, Bandyopadhyay SS, Biswas AK. Kinetics of absorption of $CO_2$ into aqueous solutions of 2-amino-2-methyl-1-propanol. *Chem Eng Sci*. 1995;50(22):3587-3598.
28. Wang L, An S, Li Q, Yu S, Wu S. Phase change behavior and kinetics of $CO_2$ absorption into DMBA/DEEA solution in a wetted-wall column. *Chem Eng J*. 2017;314:681-687.
29. Li W, Wen S, Shen L, Zhang Y, Sun C, Li S. Mechanism and kinetic study of carbon dioxide absorption into a methyldiethanolamine/1-hydroxyethyl-3-methylimidazolium lysine/water system. *Energy Fuel*. 2018;32(10):10813-10821.
30. Wang L, Yu S, Li Q, Zhang Y, An S, Zhang S. Performance of sulfolane/DETA hybrids for $CO_2$ absorption: phase splitting behavior, kinetics and thermodynamics. *Appl Energy*. 2018;228:568-576.
31. Zhou X, Shen Y, Liu F, et al. A novel dual-stage phase separation process for $CO_2$ absorption into a biphasic solvent with low energy penalty. *Environ Sci Technol*. 2021;55(22):15313-15322.
32. Naghizadeh A, Larestani A, Nait Amar M, Hemmati-Sarapardeh A. Predicting viscosity of $CO_2$–$N_2$ gaseous mixtures using advanced intelligent schemes. *J Petrol Sci Eng*. 2022;208:109359.
33. Wang T, Liu F, Ge K, Fang M. Reaction kinetics of carbon dioxide absorption in aqueous solutions of piperazine, N-(2-aminoethyl) ethanolamine and their blends. *Chem Eng J*. 2017;314:123-131.
34. Fang M, Xiang Q, Yu C, et al. Experimental study on $CO_2$ absorption by aqueous ammonia solution at elevated pressure to enhance $CO_2$ absorption and suppress ammonia vaporization. *Greenh Gases*. 2015;5(2):210-221.
35. Khan AA, Halder G, Saha AK. Kinetic effect and absorption performance of piperazine activator into aqueous solutions of 2-amino-2-methyl-1-propanol through post-combustion $CO_2$ capture. *Korean J Chem Eng*. 2019;36(7):1090-1101.
36. Wang L, Liu S, Wang R, Li Q, Zhang S. Regulating phase separation behavior of a DEEA-TETA biphasic solvent using sulfolane for energy-saving $CO_2$ capture. *Environ Sci Technol*. 2019;53(21):12873-12881.
37. Sutar PN, Vaidya PD, Kenig EY. Activated DEEA solutions for $CO_2$ capture-a study of equilibrium and kinetic characteristics. *Chem Eng Sci*. 2013;100:234-241.

38. Zheng W, Luo Q, Liu S, et al. New method of kinetic modeling for $CO_2$ absorption into blended amine systems: a case of MEA/EAE/3-DEA1P trisolvent blends. *AIChE J*. 2022;68(6):e17628.
39. Frisch MJ, Trucks GW, Schlegel HB, et al. Gaussian 09, Rev. D. 01. Gaussian, Inc. 2009.
40. Wang S, Chen Y, Jia Y, et al. Experimental and theoretical studies on glucose conversion in ethanol solution to 5-ethoxymethylfurfural and ethyl levulinate catalyzed by a Brønsted acid. *Phys Chem Chem Phys*. 2021;23(35):19729-19739.
41. Lu T, Chen F. Multiwfn: a multifunctional wavefunction analyzer. *J Comput Chem*. 2012;33(5):580-592.
42. Kierzkowska-Pawlak H, Chacuk A, Siemieniec M. Reaction kinetics of $CO_2$ in aqueous 2-(2-aminoethylamino)ethanol solutions using a stirred cell reactor. *Int J Greenh Gas Control*. 2014;24:106-114.
43. Li J, Henni A, Tontiwachwuthikul P. Reaction kinetics of $CO_2$ in aqueous ethylenediamine, ethyl ethanolamine, and diethyl monoethanolamine solutions in the temperature range of 298−313 K, using the stopped-flow technique. *Ind Eng Chem Res*. 2007;46(13):4426-4434.
44. Littel RJ, Van Swaaij WPM, Versteeg GF. Kinetics of carbon dioxide with tertiary amines in aqueous solution. *AIChE J*. 1990;36(11):1633-1640.
45. Kierzkowska-Pawlak H. Kinetics of $CO_2$ absorption in aqueous N,N-diethylethanolamine and its blend with N-(2-aminoethyl)ethanolamine using a stirred cell reactor. *Int J Greenh Gas Control*. 2015;37:76-84.
46. Benitez-Garcia J, Ruiz-Ibanez G, Al-Ghawas HA, Sandall OC. On the effect of basicity on the kinetics of $CO_2$ absorption in tertiary amines. *Chem Eng Sci*. 1991;46(11):2927-2931.
47. Kierzkowska-Pawlak H, Kruszczak E. Revised kinetics of CO 2 absorption in aqueous N, N -diethylethanolamine (DEEA) and its blend with N -methyl-1,3-propane-diamine (MAPA). *Int J Greenh Gas Control*. 2017;57:134-142.
48. Ma'mun S, Dindore VY, Svendsen HF. Kinetics of the reaction of carbon dioxide with aqueous solutions of 2-((2-aminoethyl)amino)ethanol. *Ind Eng Chem Res*. 2007;46(2):385-394.
49. Mukherjee S, Samanta AN. Kinetic study of $CO_2$ absorption in aqueous solutions of 2-((2-aminoethyl)amino)-ethanol using a stirred cell reaction calorimeter. *Int J Chem Kinet*. 2019;51(12):943-957.
50. Chen S-L, Dong P, Yang G-H, Yang J-J. Kinetics of formation of monodisperse colloidal silica particles through the hydrolysis and condensation of tetraethylorthosilicate. *Ind Eng Chem Res*. 1996;35(12):4487-4493.
51. Issa AA, Elazazy MS, Luyt AS. Polymerization of 3-cyanopropyl (triethoxy) silane: a kinetic study using gas chromatography. *Int J Chem Kinet*. 2018;50(12):846-855.
52. Orestes E, Machado Ronconi C, Carneiro JWM. Insights into the interactions of $CO_2$ with amines: a DFT benchmark study. *Phys Chem Chem Phys*. 2014;16(32):17213-17219.
53. Aso D, Orimoto Y, Higashino M, Taniguchi I, Aoki Y. Computational approach for investigating the mechanism of carbon dioxide interaction by 2-(2-aminoethylamino)ethanol: a significant role of water molecule. *Chem Phys Lett*. 2021;783:139070.
54. Wylie L, Perli G, Avila J, et al. Theoretical analysis of physical and chemical $CO_2$ absorption by tri- and tetraepoxidized imidazolium ionic liquids. *J Phys Chem B*. 2022;126(47):9901-9910.
55. Hernandez-Marin E, Lemus-Santana AA. Theoretical xtudy of the formation of complexes between $CO_2$ and nitrogen heterocycles. *J Mex Chem Soc*. 2015;59(1):36-42.
56. Hao L, Zhao Y, Yu B, et al. Imidazolium-based ionic liquids catalyzed formylation of amines using carbon dioxide and phenylsilane at room temperature. *ACS Catal*. 2015;5(9):4989-4993.


## SUPPORTING INFORMATION

Additional supporting information can be found online in the Supporting Information section at the end of this article.

**How to cite this article:** Jia R-Q, Wu Q, Zhang L-L, Zhang B, Chu G-W, Chen J-F. $CO_2$ absorption mechanism and kinetic modeling of mixed amines with ionic liquid activation. *AIChE J*. 2024;70(9):e18493. doi:10.1002/aic.18493